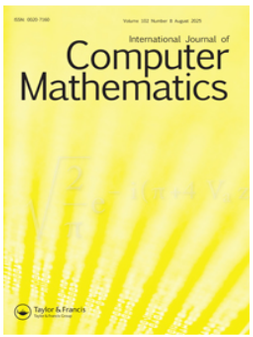

International Journal of Computer Mathematics

ISSN: 0020-7160 (Print) 1029-0265 (Online) Journal homepage: www.tandfonline.com/journals/gcom20

A new and efficient fixed point method for mean curvature denoising model

Fenlin Yang, Jianping Zhang, Jin Zhang & Ke Chen

To cite this article: Fenlin Yang, Jianping Zhang, Jin Zhang & Ke Chen (15 Jun 2025): A new and efficient fixed point method for mean curvature denoising model, International Journal of Computer Mathematics, DOI: 10.1080/00207160.2025.2517271

To link to this article: https://doi.org/10.1080/00207160.2025.2517271

Published online: 15 Jun 2025.

INTERNATIONAL JOURNAL OF COMPUTER MATHEMATICS
https://doi.org/10.1080/00207160.2025.2517271

Taylor & Francis
Taylor & Francis Group

METHOD

A new and efficient fixed point method for mean curvature denoising model

Fenlin Yang[a], Jianping Zhang[b], Jin Zhang[c] and Ke Chen[d]

[a]College of Mathematics and Statistics, Jishou University, Jishou, Hunan, People's Republic of China; [b]School of Mathematics and Computational Science, Xiangtan University, Xiangtan, Hunan, People's Republic of China; [c]School of Mathematical Sciences, Liaocheng University, Liaocheng, People's Republic of China; [d]Department of Mathematics and Statistics, University of Strathclyde, Glasgow, United Kingdom

ABSTRACT

The mean curvature model is one of the efficient higher-order models for image denoising, and its Euler-Lagrange equation is a fourth-order nonlinear equation which makes the development of efficient numerical methods very difficult. In this paper, on the one hand, it is proposed to replace the gradient in the nonlinear terms other than the mean curvature with the gradient obtained by convolving the image with a Gaussian low-pass filter. This modification leads to a new Euler-Lagrange equation that retains the structure of the original equation, but with a reduced degree of nonlinearity. On the other hand, we also develop a novel fixed point curvature method to solve this new equation. Numerical experiments show that our method not only recovers high-quality images from highly noisy images, but is also 10 times faster than the nonlocal means (NLM) method and 6–10 times faster than the the augmented Lagrangian method.

ARTICLE HISTORY
Received 29 September 2024
Revised 16 January 2025
Accepted 2 June 2025

KEYWORDS
Image denoising; mean curvature; Gaussian low-pass filter; fixed point method; Euler-Lagrange equation

2020 MATHEMATICS SUBJECT CLASSIFICATIONS
65K10; 90C30; 90C47; 35G20

1. Introduction

Inverse problems arise from various fields in applied sciences and engineering challenges. Typically, a mathematical model modeling an inverse problem includes data fidelity and regularization; the former varies with the problem, while the latter overcomes the ill-posed nature of an inverse problem by limiting the solution space. This paper presents a novel and efficient algorithm for a high-order model based on the mean curvature regularizer. Although it can be applied to numerous models [26,29,36], we focus specifically on the image noise removal problem.

Let u be a true and unknown image and η be some random noise. In the scenario of additive Gaussian noise, given an observed image z, our goal is to restore u from

$$z = u + \eta. \tag{1}$$

There exist several other noise models, including multiplicative noise [16], Poisson noise [18], Cauchy noise [1,14] and Rican noise [31]. However, the fidelity of these noise models varies. Analyzing the previously mentioned model (1) is sufficient without loss of generality. The goal of image denoising is to remove noise η while preserving key features in u such as edges.

CONTACT Ke Chen k.chen@strath.ac.uk, https://personal.strath.ac.uk/k.chen/ Department of Mathematics and Statistics, University of Strathclyde, Glasgow G1 1XQ, United Kingdom

This paper is concerned with an effective solution for the variational model to solve (1)

$$\min_u \left\{ J(u) = \alpha \int_\Omega \Phi(\kappa)\, \mathrm{d}x\mathrm{d}y + \frac{1}{2}\|u - z\|^2_{L^2(\Omega)} \right\}, \tag{2}$$

where the non-negative function $\Phi(\cdot)$ is defined either as $\Phi(\kappa) = |\kappa|$, $\Phi(\kappa) = \kappa^2/2$, or a combination of both. Here the most important geometric quantity is the mean curvature

$$\kappa = \nabla \cdot \frac{\nabla u}{\sqrt{1 + |\nabla u|^2}},$$

which is more effective in (2) compared to other regularization methods. However, the model (2) is known to be extremely challenging to solve. This paper addresses this challenge by developing a new reformulation and, consequently, a new numerical method.

Many related works have been proposed and investigated for (1). The total variation (TV) model, introduced by Rudin, Osher, and Fatemi [23], is widely used in image processing due to its effectiveness as a low-order convex model to preserve the edges and contours of objects. In addition, several fast and efficient numerical methods are available [7,8,28]. However, the model exhibits staircase effects, blurs object corners, and fails to preserve intensity contrasts. In [21], Osher, Solé and Vese proposed to use the H^{-1} norm for the oscillatory functions as the fitting term to preserve the texture within the TV model, referred to as the following OSV model

$$\min_u \alpha \int_\Omega |\nabla u| \mathrm{d}x\mathrm{d}y + \frac{1}{2}\int_\Omega |\nabla(\Delta^{-1})(u - z)|^2 \mathrm{d}x\mathrm{d}y.$$

The corresponding Euler-Lagrange equation transformed by the Laplace operator is

$$\alpha\Delta\left(\nabla \cdot \frac{\nabla u}{|\nabla u|}\right) + (u - z) = 0, \quad \left.\frac{\partial u}{\partial \vec{n}}\right|_{\partial\Omega} = 0, \quad \left.\frac{\partial \kappa}{\partial \vec{n}}\right|_{\partial\Omega} = 0, \tag{3}$$

where $\partial\Omega$ is the boundary of the domain Ω, $\vec{n}$ is outer normal vector.

Over the last two decades, several high-order models [3,9,10,17,39] have been developed to address these undesirable properties and achieve satisfactory results. One of the most famous high-order models was first studied by Zhu-Chan [39], whose time marching method was found to be excessively slow. However, this model improves the staircase effects found in the TV model while preserving image contrast and object edge sharpness. To illustrate the difficulty, consider $\Phi(\kappa) = \kappa^2/2$ as an example: the corresponding Euler-Lagrange equation is non-trivial and takes the form

$$g(u) = \alpha\nabla \cdot \frac{1}{\sqrt{1 + |\nabla u|^2}}\left(\boldsymbol{I} - \frac{\nabla u \nabla u^T}{1 + |\nabla u|^2}\right)\nabla\kappa + (u - z) = 0, \quad (x, y) \in \Omega \tag{4}$$

with the same boundary condition of (3), where $\boldsymbol{I} \in \mathbf{R}^{2\times 2}$ is the identity matrix. The time marching approach is quite slow because it has to satisfy the CFL condition by choosing a small time step. Also, certain methods that were effective for the TV model, such as lagged fixed point methods [28] and primal-dual methods [8], do not work for (4), as shown in [4].

An effective approach for this mean curvature model, $\Phi(\kappa) = |\kappa|$, is the augmented Lagrangian methods (ALM) [35,37,38], which achieve approximations of the minimizers of the original high-order functional by focusing on minimizing multiple low-order functionals. While augmented Lagrangian methods are increasingly refined for dealing with high order variational models [11–13,15,26,34], tuning the hyper-parameters becomes complex and challenging. Furthermore, the interactions among the decoupled variables become complicated due to the integration of multiple intermediate variables and parameters. In addition, establishing theoretical convergence is difficult due to the complex interdependencies among the auxiliary variables.

To avoid introducing multiple intermediate variables, Brito-Loeza and Chen [4] present an efficient nonlinear multigrid which uses the stabilized fixed point method as a smoother. In [32], the authors proposed a homotopy method based on gradually decreasing the smoothing parameter β to provide a good initial value for the fixed point curvature method.

In this study, we use Gaussian low-pass filtering to suppress the peaks of the gradient beyond the mean curvature in the nonlinear part of the Euler-Lagrange Equation (4) in order to reduce the nonlinearity. For simplicity, the resulting approximate equation is called the new Euler-Lagrange equation, and the degree of nonlinearity can be varied by varying the standard deviation σ of the Gaussian filter. Although the lagged fixed point method cannot solve (4), it can solve the new Euler-Lagrange equation as long as σ is large enough. This is crucial for the success of the new method.

The rest of this paper is organized as follows. In Section 2, we will present the work related to the algorithms in this paper in terms of both the combination of filtering and PDEs, and the fixed point curvature method. In Section 3, we give the formulation of the new Euler-Lagrange equation by analyzing the second-order semipositive definite operator and construct a fixed-point method for solving the new Euler-Lagrange equation. In Section 4, we present various numerical results obtained from the implementation of the proposed algorithm.

2. The related works

We give a brief review of previous methods that are designed to reduce nonlinearity or to facilitate better decoupling.

Traditional denoising methods mainly rely on local filtering or least-squares estimation. Although these methods are straightforward and can extract the trend of the signal, they result in edge blurring and do not preserve the details and contrast of the image.

In image processing, the method of incorporating low-pass filtering into partial differential equations (PDEs) has long been used. Torre and Poggio [27] provide a thorough validation for the application of filtering before differentiation by analysing the properties of different integro-differential operators proposed for edge detection. As noted by Witkin [30], applying a Gaussian convolution to the signal at each scale is equivalent to solving the heat equation with the signal as the initial condition. Malik and Perona [22] proposed a model for edge detection by anisotropic diffusion defined by

$$\frac{\partial u}{\partial t} = \nabla \cdot \left(f(|\nabla u|) \nabla u \right), \quad u^{(0)} = G_\sigma * z. \tag{5}$$

where $f(\cdot) : \mathbb{R}^+ \to [0, 1]$ is a smooth decreasing function with $f(0) = 1$, and $f(|\nabla u|) \to 0$ ($|\nabla u| \to \infty$). To reduce irrelevant peaks in the gradient due to noise, the initial smoothing of z is performed with a low-pass filter G_σ. This approach appears to reintroduce the nonadaptive filtering that the theory initially sought to avoid, resulting in a loss of edge accuracy.

The modification of the model (5) suggested in [6] involves substituting $|\nabla u|$ with its approximation $|\nabla G_\sigma * u|$ to avoid the inconsistencies in the Perona and Malik model as demonstrated below

$$\frac{\partial u}{\partial t} = \nabla \cdot \left(f(|\nabla G_\sigma * u|) \nabla u \right), \quad u^{(0)} = z. \tag{6}$$

However, this model does not have a clear geometric interpretation.

Based on the geometric interpretation of $|\nabla u|\kappa$ which diffuses u in the tangential direction but not in the normal direction at all [19,20], the mean curvature motion model

$$\frac{\partial u}{\partial t} = |\nabla u| \nabla \cdot \frac{\nabla u}{|\nabla u|}, \quad u^{(0)} = z \tag{7}$$

has received significant attention in image processing. Alvarez, Lions and Morel [2] combined the geometric interpretation of mean curvature motion with the Perona and Malik theory to propose the

nonlinear parabolic differential equation

$$\frac{\partial u}{\partial t} = f(|\nabla G_\sigma * u|)|\nabla u|\nabla \cdot \frac{\nabla u}{|\nabla u|}, \quad u^{(0)} = z. \tag{8}$$

The fixed point technique proposed by Vogel and Omen [28] can be formulated as a quasi-Newton iterative scheme. Conversely, the authors in [7] propose that it can be viewed as a semi-implicit time-stepping approach with an infinite time step. Inspired by the quasi-Newton structure of the fixed point method, we develop a fixed point curvature technique [32] to solve the MC model with a large positive parameter β. This technique is less nonlinear, and the quasi-Newton method shows a wider range of convergence. Since the fourth order nonlinear term is a second-order nonlinear operator acting on another second-order nonlinear term, the current known iteration $u^{(k)}$ ($u^{(0)} = z$) is employed to fix the outer second-order operator defined by

$$\mathcal{M}(\nabla u) = -\nabla \cdot \frac{1}{\sqrt{|\nabla u|^2 + \beta}} \left(\boldsymbol{I} - \frac{\nabla u \nabla u^T}{|\nabla u|^2 + \beta} \right) \nabla,$$

resulting in a simplified nonlinear equation

$$-\alpha \mathcal{M}(\nabla u^{(k)}) \nabla \cdot \frac{\nabla u}{\sqrt{|\nabla u|^2 + \beta}} + (u - z) = 0, \tag{9}$$

which similar to the Euler-Lagrange equation of TV model. Therefore, the next iteration for updating $\mathcal{M}(\nabla u)$ is achieved through the lagged fixed point method. A homotopy equation is formulated where the parameter β is gradually reduced to 1, applying this fixed point curvature approach as a correction mechanism in path tracking.

In [33], a relaxed fixed point (RFP) method is proposed, which reduces the nonlinearity of (4) by removing the highly nonlinear term from $\mathcal{M}(\nabla u)$, i.e. replacing $\mathcal{M}(\nabla u)$ with $-\nabla \cdot \frac{1}{\sqrt{|\nabla u|^2+\beta}} \nabla$. The method produces high quality denoised images, although it is not a direct solution of the Euler-Lagrange Equation (4).

3. A new fixed point curvature method

As observed by Brito-Loeza and Chen [4], the variations of directly constructed fixed point methods are ineffective for the mean curvature model. A significant reformulation is necessary to make the Equation (4) suitable for the development of a fixed point method.

In this study, the gradient ∇u within $\mathcal{M}(\nabla u)$ is replaced by $\nabla G_\sigma * u$ to reduce the peak of the gradient and thus the nonlinearity of $\mathcal{M}(\nabla u)$. A fixed point iterative approach is then formulated to solve the new Euler-Lagrange equation.

3.1. Motivation

Our previous work [32], which applied a homotopy method involving the gradual reduction of the parameter β as illustrated in (9), gave very encouraging experimental results. To provide a basis for our new study, we present below a brief analysis. First, we define

$$\mathcal{D}(\nabla u) = \frac{1}{\sqrt{|\nabla u|^2 + \beta}} \left(\boldsymbol{I} - \frac{\nabla u \nabla u^T}{|\nabla u|^2 + \beta} \right) = \frac{1}{(|\nabla u|^2 + \beta)^{\frac{3}{2}}} \begin{pmatrix} u_y^2 + \beta & -u_x u_y \\ -u_x u_y & u_x^2 + \beta \end{pmatrix},$$

and then denote $\mathcal{M}(\nabla u) = -\nabla \cdot (\mathcal{D}(\nabla u)\nabla)$. It is not difficult to prove the following two propositions.

Proposition 3.1: *For any $\beta > 0$, the matrix $\mathcal{D}(\nabla u)$ is a symmetric positive definite matrix with two eigenvalues*

$$\lambda_1 = \frac{1}{\sqrt{|\nabla u|^2 + \beta}}, \quad \lambda_2 = \frac{\beta}{\left(|\nabla u|^2 + \beta\right)^{\frac{3}{2}}} = \frac{\beta}{|\nabla u|^2 + \beta}\lambda_1 \leq \lambda_1,$$

and the condition number is

$$Cond(\mathcal{D}(\nabla u)) = \frac{\lambda_1}{\lambda_2} = \frac{|\nabla u|^2 + \beta}{\beta}.$$

Proposition 3.2: *The diagonal matrix of $\mathcal{D}(\nabla u)$ satisfies*

$$\frac{\beta}{\left(|\nabla u|^2 + \beta\right)^{\frac{3}{2}}}\boldsymbol{I} \leq \frac{1}{(|\nabla u|^2 + \beta)^{\frac{3}{2}}}\begin{pmatrix} u_y^2 + \beta & 0 \\ 0 & u_x^2 + \beta \end{pmatrix} \leq \frac{1}{\sqrt{|\nabla u|^2 + \beta}}\boldsymbol{I}.$$

If β is large enough and $|\nabla u|$ is finite, then we have $-u_x u_y/(|\nabla u|^2 + \beta)^{\frac{3}{2}}$ and $\sqrt{|\nabla u|^2 + \beta}$ are close to 0 and $\sqrt{\beta}$ respectively. According to the Proposition 3.2, $\mathcal{D}(\nabla u)$ will be close enough to the matrix $\frac{1}{\sqrt{\beta}}\boldsymbol{I}$. Since

$$-\nabla \cdot \left(\frac{1}{\sqrt{\beta}}\boldsymbol{I}\nabla\right) = -\frac{1}{\sqrt{\beta}}\nabla \cdot \nabla = -\frac{1}{\sqrt{\beta}}\Delta,$$

the Equation (9) is close to (3). It is known that an OSV model with an appropriate regularization parameter is effective not only in removing noise but also in preserving texture; however, a large β results in a small regularization parameter and the iterative solution remains close to the noisy image. Therefore, using a homotopy technique with a decreasing β for path tracking results in an increasing regularization parameter as β decreases, which removes more noise and subsequently reduces the peak value of the noise-induced gradient uncorrelation.

The key to developing algorithms for solving (4) is to reduce the nonlinearity. Both of the above methods focus on reducing the nonlinearity of $\mathcal{M}(\nabla u)$. The fixed point curvature technique requires extending a significant parameter β to 1, while the RFP approach removes the highly nonlinear term in (4). In particular, as the condition number $\mathcal{D}(\nabla u)$ decreases, so does the nonlinearity of $\mathcal{M}(\nabla u)$. So we set $\beta = 1$, so that $\text{Cond}(\mathcal{D}(\nabla u)) = 1 + |\nabla u|^2$ depends only on $|\nabla u|$, which leads us to try to reduce $\text{Cond}(\mathcal{D}(\nabla u))$ by reducing $|\nabla u|$.

Witkin [30] observes that convolving a signal with a Gaussian at each scale $\sqrt{\sigma}$, represented as $u(x, y, \sigma) = G_\sigma * u^{(0)}(x, y)$, corresponds to solving the heat equation

$$\frac{\partial u(x, y, \sigma)}{\partial \sigma} = \Delta u(x, y, \sigma), \quad u(x, y, 0) = u^{(0)}(x, y).$$

The Gaussian convolution kernel function is symmetric and strictly decreasing around the mean, ensuring that the weights decrease smoothly with increasing distance. For a small standard deviation σ, the Gaussian convolution $G_\sigma * u$ approximates u; for a large σ, $G_\sigma * u$ approximates the mean of u. In general, $|\nabla G_\sigma * u|$ is less than $|\nabla u|$, and $|\nabla G_\sigma * u|$ gradually approaches zero as σ increases.

3.2. Formulation of the new Euler-Lagrange equation

Due to the noise, the gradient of the image undergoes extremely large and theoretically infinite oscillations. When the noisy image z is used as the initial value in the fixed point curvature method, the uncorrelated peak of the noise-induced gradient leads to a significantly large $\text{Cond}(\mathcal{D}(\nabla z))$. Note

that $\mathcal{D}(\nabla z)$ is the matrix constructed by ∇z, and its condition number is $1 + |\nabla z|^2$. By replacing ∇z in $\mathcal{D}(\nabla z)$ with $\nabla G_\sigma * z$, we get

$$\mathrm{Cond}(\mathcal{D}(\nabla G_\sigma * z)) = 1 + |\nabla G_\sigma * z|^2 \leq 1 + |\nabla z|^2 = \mathrm{Cond}(\mathcal{D}(\nabla z)).$$

Even in cases where σ is so large that $\mathcal{M}(\nabla G_\sigma * z)$ approaches the Laplace operator Δ, the texture preserving properties of the OSV model will not cause excessive blurring of the image edges. Furthermore, changing σ does not affect the α regularization parameter.

Based on the above analysis, we replace $\mathcal{M}(\nabla u)$ by $\mathcal{M}(\nabla G_\sigma * u)$ to obtain the following new Euler-Lagrange equation

$$\tilde{g}(u) = -\alpha \mathcal{M}(\nabla G_\sigma * u)\nabla \cdot \frac{\nabla u}{\sqrt{1 + |\nabla u|^2}} + (u - z) = 0. \tag{10}$$

Note that the nonlinear term of (10) integrates a second order symmetric positive semidefinite operator $\mathcal{M}(\nabla G_\sigma * u)$ with the mean curvature κ, which is an important geometric quantity with nonlinear structure, and its nonlinearity is less than that of $\mathcal{M}(\nabla u)\kappa$.

3.3. The fixed point iterative method for (eqn10)

We have justified the validity of the new Euler-Lagrange Equation (10). Next, we look at how to solve this fourth-order nonlinear equation.

Newton's method is known to be a fast iterative method for solving nonlinear equations. However, Newton's method cannot be directly applied to standard TV models or to this particular equation.

Proposition 3.3: *Suppose $u^{(k)}$ is known. Given that $\mathcal{D}(\nabla G_\sigma * u^{(k)}) \in R^{2\times 2}$ is a symmetric positive definite matrix, then the semi-positive operator $\mathcal{M}(\nabla G_\sigma * u^{(k)}) = -\nabla \cdot \mathcal{D}(\nabla G_\sigma * u^{(k)})\nabla$. Consequently, the equation*

$$-\alpha \mathcal{M}(\nabla G_\sigma * u^{(k)})\nabla \cdot \frac{\nabla u}{\sqrt{1 + |\nabla u|^2}} + (u - z) = 0$$

is equivalent to

$$\alpha \nabla \cdot \frac{\nabla u}{\sqrt{1 + |\nabla u|^2}} - \left(\mathcal{M}(\nabla G_\sigma * u^{(k)})\right)^{-1}(u - z) = 0, \tag{11}$$

which represents the optimality condition for minimizing the following energy functional:

$$\alpha \int_\Omega |\nabla u|_1 \mathrm{d}x\mathrm{d}y + \frac{1}{2}\int_\Omega \left| \mathcal{D}(\nabla G_\sigma * u^{(k)})^{\frac{1}{2}} \nabla \left(\mathcal{M}(\nabla G_\sigma * u^{(k)})\right)^{-1}(u - z)\right|^2 \mathrm{d}x\mathrm{d}y. \tag{12}$$

In [24], Shi, Chang, and Xu established the convergence of the fixed-point method for the TV image deblurring model:

$$\alpha \int_\Omega |\nabla u|_\beta \mathrm{d}x\mathrm{d}y + \frac{1}{2}\int_\Omega |Ku - z|^2 \mathrm{d}x\mathrm{d}y, \tag{13}$$

where K denotes the blurring operator. Since both the second terms in Equations (15) and (16) are convex, the fixed point method for (11) with the initial value $u^{(0)} = z$ is convergent. This can be

formally written as follows:

$$-\alpha\nabla\cdot\frac{\nabla u^{(k+1)}}{\sqrt{1+|\nabla u^{(k)}|^2}}+\left(\mathcal{M}(\nabla G_\sigma * u^{(k)})\right)^{-1}(u^{(k+1)}-z)=0,\quad k=0,1,2,\ldots$$

which can be rewritten as follows

$$-\alpha\mathcal{M}(\nabla G_\sigma * u^{(k)})\nabla\cdot\frac{\nabla u^{(k+1)}}{\sqrt{1+|\nabla u^{(k)}|^2}}+(u^{(k+1)}-z)=0,\quad k=0,1,2,\ldots \tag{14}$$

The fixed point method described above can be considered as a semi-implicit time marching method with an infinite time step. As the Equation (10) is still fourth order nonlinear equation, this fixed point method is still slow to converge.

Taking the current iteration $u^{(k)}$ as the approximate solution of (10), then $-\tilde{g}(u^{(k)})$ is the residual of (10). The residual equation of (10) is as follows

$$\left(-\alpha\mathcal{M}(\nabla G_\sigma * u^{(k)})\nabla\cdot\frac{\nabla}{\sqrt{1+|\nabla u^{(k)}|^2}}+1\right)e^{(k)}=-\tilde{g}(u^{(k)}). \tag{15}$$

where $e^{(k)}$ is the error that needs to be solved, and the next iteration is $u^{(k+1)}=u^{(k)}+e^{(k)}$.

In fact, by simply moving the right term of Equation (15) to the left, we have

$$\begin{aligned}0&=-\alpha\mathcal{M}(\nabla G_\sigma * u^{(k)})\nabla\cdot\frac{\nabla e^{(k)}}{\sqrt{1+|\nabla u^{(k)}|^2}}+e^{(k)}+\tilde{g}(u^{(k)})\\&=-\alpha\mathcal{M}(\nabla G_\sigma * u^{(k)})\nabla\cdot\frac{\nabla\left(u^{(k)}+e^{(k)}\right)}{\sqrt{1+|\nabla u^{(k)}|^2}}+\left(u^{(k)}+e^{(k)}-z\right)\\&=-\alpha\mathcal{M}(\nabla G_\sigma * u^{(k)})\nabla\cdot\frac{\nabla u^{(k+1)}}{\sqrt{1+|\nabla u^{(k)}|^2}}+\left(u^{(k+1)}-z\right).\end{aligned}$$

The above analysis is based on the case where $u^{(k+1)}$ and $e^{(k)}$ are analytical solutions of Equations (14) and (15) respectively. However, we can only find numerical solutions for the fourth order Equations (14) and (15), so $u^{(k+1)}$ is not really the same as $u^{(k)}+e^{(k)}$. (15) can be considered as a fixed point method of quasi-Newton form, the efficiency of the algorithm can be improved by applying (15), since the quasi-Newton method generally has superlinear convergence.

We will now present the discretisation of the continuous formulation of the Euler-Lagrange equation for the MC model in $\Omega=[0,n]\times[0,n]$. The mesh size is $d=1$, and $u_{i,j}$ $(i,j=1,2,\ldots,n)$ denotes the value of the function u at pixel (i,j). Then the forward difference of gradient at pixel (i,j) is defined by

$$(\nabla u)_{i,j}=\left((u_x)_{i,j};(u_y)_{i,j}\right)$$

with

$$(u_x)_{i,j}=\begin{cases}u_{i+1,j}-u_{i,j} & \text{if } i<n,\\ 0 & \text{if } i=n,\end{cases}\qquad (u_y)_{i,j}=\begin{cases}u_{i,j+1}-u_{i,j} & \text{if } j<n,\\ 0 & \text{if } j=n.\end{cases}$$

Since the divergence operator is the negative adjoint of the gradient operator, i.e. $\nabla\cdot = -\nabla^*$. Therefore, the discrete divergence operator can be defined as follows

$$(\nabla\cdot\nabla u)_{i,j} = \begin{cases} (u_x)_{i,j} & \text{if } i = 1 \\ (u_x)_{i,j} - (u_x)_{i-1,j} & \text{if } i = 2,\ldots,n \\ -(u_x)_{i-1,j} & \text{if } i = n \end{cases} + \begin{cases} (u_y)_{i,j}, & \text{if } j = 1, \\ (u_y)_{i,j} - (u_y)_{i,j-1}, & \text{if } j = 2,\ldots,n, \\ -(u_y)_{i,j-1}, & \text{if } j = n. \end{cases}$$

To simplify the notation, we use bold letters to represent the vector. Once we have stacked the grid function u along the rows of Ω into a vector

$$\mathbf{u} = (u_{1,1},\ldots,u_{n,1},u_{1,2},\ldots,u_{n,2},\ldots,u_{1,n},\ldots,u_{n,n})^T$$

as usual, then $\mathbf{u}\in\mathbf{R}^N$, where $N = n^2$. Let $v = G_\sigma * u$, then $\mathbf{v}$ denotes the transformation of $G_\sigma * u$ into vectors along the rows of Ω.

The discrete gradient $(\nabla u)_{i,j}$ can be expressed by multiplying the matrix $A_l^T\in\mathbf{R}^{2\times N}$, for $l = 1,2,\ldots,N$, into the vector $\mathbf{u}$:

$$A_l^T\mathbf{u} = \begin{cases} (\mathbf{u}_{l+1} - \mathbf{u}_l; \mathbf{u}_{l+n} - \mathbf{u}_l), & \text{if } l \bmod n \neq 0 \text{ and } l+n \leq N, \\ (0; \mathbf{u}_{l+n} - \mathbf{u}_l), & \text{if } l \bmod n = 0 \text{ and } l+n \leq N, \\ (\mathbf{u}_{l+1} - \mathbf{u}_l; 0), & \text{if } l \bmod n \neq 0 \text{ and } l+n > N, \\ (0;0), & \text{if } l \bmod n = 0 \text{ and } l+n > N. \end{cases}$$

It can be deduced that the discretisation of (15) is

$$(\alpha\mathcal{M}_1\mathcal{M}_2 + \boldsymbol{I}_N)\,\mathbf{e}^{(k)} = -\tilde{g}(\mathbf{u}^{(k)}), \tag{16}$$

where

$$\mathcal{M}_1 = \sum_i A_i \frac{1}{\sqrt{1+|A_i^T\mathbf{v}^{(k)}|^2}}\left(\boldsymbol{I} - \frac{A_i^T\mathbf{v}^{(k)}\bigotimes(A_i^T\mathbf{v}^{(k)})^T}{1+|A_i^T\mathbf{v}^{(k)}|^2}\right)A_i^T, \quad \mathcal{M}_2 = \sum_i A_i \frac{A_i^T}{\sqrt{1+|A_i^T\mathbf{u}^{(k)}|^2}}.$$

Here $\bigotimes$ denotes the Kronecker product and $\boldsymbol{I}_N$ is a unit matrix of dimension N. Note that $\mathcal{M}_1, \mathcal{M}_2 \in R^{N\times N}$ are non-diagonal symmetric semipositive definite matrices, so their product $\mathcal{M}_1\mathcal{M}_2$ is an asymmetric semipositive definite matrix [32].

Proposition 3.4: *The Conjugate Gradient Squaring (CGS) method proposed in* [25] *is a polynomial-based conjugate gradient algorithm for systems of asymmetric sparse linear equations. Since the coefficient matrix $\alpha\mathcal{M}_1\mathcal{M}_2 + \boldsymbol{I}_N$ of linear Equations* (16) *is an asymmetric positive definite sparse matrix, the solution of* (15) *by the CGS method will converge.*

The FPC1 method described below is intended for images with low levels of noise, where no new intermediate variables are introduced and only a parameter σ is added.

Algorithm 1: $[\mathbf{u}, k] \leftarrow FPC1(\mathbf{z}, k_{\max}, tol, \sigma)$

step 1. *Set* $k = 0, \mathbf{u}^{(k)} = \mathbf{z}$.

step 2. *While* $k < k_{\max}$, *do Compute* $\alpha\mathcal{M}_1\mathcal{M}_2 + \boldsymbol{I}_N$ *and* $\tilde{g}(\mathbf{u}^{(k)})$, *using the CGS method, find the solution of (16), set* $\mathbf{u}^{(k+1)} = \mathbf{u}^{(k)} + \mathbf{e}^{(k)}$, $k = k + 1$. *If* $\|\mathbf{e}^{(k)}\| < tol$, *return with* $\mathbf{u} = \mathbf{u}^{(k)}$, *break.*

step 3. *Return with* $\mathbf{u} = \mathbf{u}^{(k)}$.

For images with high noise, it is necessary to increase the σ of the Gaussian filter to effectively minimize the uncorrelated maximum of the noise gradient. However, a larger σ would cause (10) to approximate (3). To solve this problem, we propose a stepwise reduction of the standard deviation σ in the FPC1 method. The algorithm is as follows.

Algorithm 2: $[\mathbf{u}, k] \leftarrow FPC2(\mathbf{z}, k_{\max}, tol, \sigma_0, \sigma)$

step 1. *Set* $k = 0, \mathbf{u}^{(k)} = \mathbf{z}, \sigma_k = \sigma_0$.

step 2. *While* $\sigma_k > \sigma$, *do*

(i) Compute the $\alpha\mathcal{M}_1\mathcal{M}_2 + \boldsymbol{I}_N$ *and* $\tilde{g}(\mathbf{u}^{(k)})$, *using the CGS method, find the solution of (16), set* $\mathbf{u}^{(k+1)} = \mathbf{u}^{(k)} + \mathbf{e}^{(k)}$.

(ii) Choose $\sigma_{k+1} < \sigma_k$, $k = k + 1$.

step 3. *While* $\|\mathbf{e}^{(k)}\| > tol$ *and* $k < k_{\max}$, *do Compute* $\alpha\mathcal{M}_1\mathcal{M}_2 + \boldsymbol{I}_N$ *and* $\tilde{g}(\mathbf{u}^{(k)})$, *using the CGS method, find the solution of (16), set* $\mathbf{u}^{(k+1)} = \mathbf{u}^{(k)} + \mathbf{e}^{(k)}$, $k = k + 1$.

step 4. *Return with* $\mathbf{u} = \mathbf{u}^{(k)}$.

4. Numerical experiments and discussions

The effectiveness of the model (2) and a lack of efficient methods are widely discussed. In this section, our main goal is to demonstrate the superior efficiency of our newly developed method. We employ both synthetic and natural images with intensity levels ranging from [0, 255] to evaluate our proposed methods. Gaussian white noise, with a mean of zero and standard deviations of 10, 20, and 30, is introduced to the original images of various pixels. All numerical experiments are executed using MATLAB on a Windows 10 (64bit) notebook with a 1.60 GHz Intel(R) Core(TM) i5-10210U CPU and 8GB of RAM.

To quantitatively assess the quality of the restored images at various noise levels, we employed the signal-to-noise ratio (SNR), and structural similarity index measure (SSIM). The definitions of SNR, and SSIM are as follows:

$$\mathrm{SNR} = 10\log_{10}\frac{\sum_{i=1}^{n}\sum_{j=1}^{n}\tilde{u}_{i,j}^2}{\sum_{i=1}^{n}\sum_{j=1}^{n}(u_{i,j}-\tilde{u}_{i,j})^2}, \quad \mathrm{SSIM} = \frac{(2\mu_{\tilde{u}}\mu_u + c_1)(2\sigma_{\tilde{u}u} + c_2)}{(\mu_{\tilde{u}}^2 + \mu_u^2 + c_1) + (\sigma_{\tilde{u}}^2 + \sigma_u^2 + c_2)},$$

where $\tilde{u}$ represents the original image and u represents the restored image, $\mu_{\tilde{u}}$ and μ_u are the local mean values of the images $\tilde{u}$ and u, $\sigma_{\tilde{u}}$ and σ_u are their respective standard deviations; c_1 and c_2 are constants to prevent the denominator from approaching zero; and $\sigma_{\tilde{u}u}$ is the covariance between $\tilde{u}$ and u.

4.1. The performance of the new fixed point curvature method

In this experiment we use test images with a noise level of 10. Firstly, we test the changes in SNR and relative residual ($\mathrm{ReRes} = \|g(\tilde{\mathbf{u}})\|_2/\|g(\mathbf{z})\|_2$) with increasing the number of iterations of the FPC1 method; secondly, we compare the HMTP [32] and RFP [33] methods with the FPC1 method for images at different pixels. In general, the denoising result depends mainly on the regularization parameter α. The α parameters for 'Circle', 'Synthetic', 'Pepper' and 'Aircraft' are 150, 200, 100 and 100 respectively, and $\sigma = 1.2$.

The SNR and SSIM of the recovered images from the HMTP method, the RFP method and the FPC1 method, as well as the CPU time (in seconds), are shown in Table 1. From Table 1 it can be seen

Table 1. Numerical results for test images with a noisy of 10.

pixels		256×256			512×512			1024×1024		
Example	Method	SNR	SIMM	time	SNR	SIMM	time	SNR	SIMM	time
Circle	HMTP	30.5	0.9726	66.1	31.1	0.9835	237	32.3	0.9901	1113
	RFP	31.4	0.9858	24.9	33.2	0.9917	107	35.3	0.9929	441
	FPC1	31.7	0.9864	5.6	33.8	0.9918	36.9	35.5	0.9928	128
Synthetic	HMTP	35.8	0.9846	49.5	38.3	0.9916	238	40.2	0.9939	1802
	RFP	36.4	0.9913	25.1	39.0	0.9937	139	41.8	0.9945	551
	FPC1	37.2	0.9906	6.2	39.4	0.9938	27.5	41.7	0.9944	121
Pepper	HMTP	27.0	0.8985	83.5	27.0	0.9349	311	28.1	0.9685	1443
	RFP	27.5	0.9239	22.3	28.3	0.9556	129	30.2	0.9784	469
	FPC1	28.2	0.9350	4.7	28.6	0.9599	32.8	30.3	0.9796	147
Aircraft	HMTP	27.9	0.9156	47.2	28.8	0.9470	224	29.5	0.9716	1684
	RFP	28.9	0.9690	36.1	30.4	0.9790	180	32.5	0.9866	575
	FPC1	29.4	0.9695	5.3	31.1	0.9798	25.9	33.0	0.9863	141

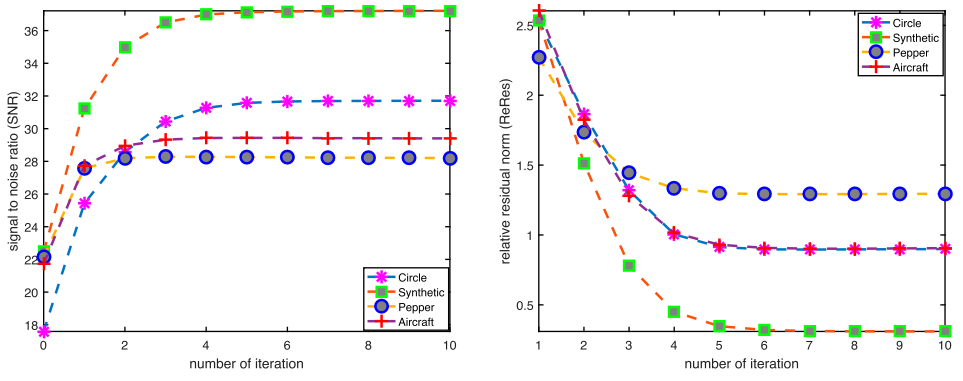

Figure 1. Description of the SNR (left) and ReRes (right) for images of size 256 × 256 in FPC1 iterations.

that the FPC1 method has the shortest CPU time, approximately one tenth of the HMTP method and one quarter of the RFP method. Furthermore, the FPC1 method yields the highest SNR in the recovered images, with a 1.0–3.5 dB improvement over the HMTP method and a 0.2–0.8 dB improvement over the RFP method. The SSIM values for the recovered images using both the FPC1 and RFP methods are also well above those of the HMTP method.

Figures 1 describe the SNR and ReRes in fixed point iterations. The left figure shows that the SNR increases with the number of iterations, with the first four iterations growing rapidly and the fifth iteration starting to slow down, the SNR of the synthetic image grows close to 15 dB and the SNR of the natural image grows close to 8 dB. The right-hand figure shows that the ReRes value of both the synthetic and natural images decreases as the number of iterations increases and tends to stabilize after the fifth iteration.

4.2. Comparison of OSV, NLM and FPC2 methods

The NLM method [5], which uses the average of all points in a Gaussian neighborhood similar to the (x, y) neighborhood as the denoising value at (x, y), is an improvement on the traditional local filtering method. It is able to preserve the detailed features of the image. In this numerical experiment, we compare the OSV method and the NLM method with the FPC2 method. Gaussian white noise with zero mean and 30 variance is added to the original images. The α parameters for 'Synthetic', 'Pepper' and 'Aircraft' are 750, 400 and 400 respectively, and $\sigma_0 = 10, \sigma = 2$. The SNR and SSIM of the recovered image and the computation time (in seconds) are shown in the Table 2. In this experiment, we

Table 2. Numerical results for images with a noisy level 30.

pixels		256×256			512×512			1024×1024		
Example	Method	SNR	SSIM	time	SNR	SSIM	time	SNR	SSIM	time
Synthetic	OSV	30.6	0.9672	5.83	33.2	0.9707	31.8	35.3	0.9684	144
	NLM	30.2	0.8927	63.6	31.5	0.9622	332	31.9	0.9771	1175
	FPC2	30.7	0.9717	6.82	33.2	0.9803	33.4	35.2	0.9773	119
Pepper	OSV	21.8	0.8504	4.13	23.3	0.9047	20.1	26.9	0.9441	112
	NLM	21.9	0.8122	63.1	24.1	0.8907	270	26.3	0.9425	1400
	FPC2	22.4	0.8506	6.95	24.2	0.9103	33.6	26.6	0.9491	119
Aircraft	OSV	20.7	0.8912	3.62	22.3	0.9294	23.0	26.3	0.9437	112
	NLM	22.6	0.8688	64.2	25.0	0.9408	283	27.1	0.9664	1199
	FPC2	22.6	0.9199	9.08	25.0	0.9541	30.6	27.3	0.9627	121

set the search window to 21 × 21 pixels and a similarity square neighborhood window to 7 × 7, and the filter parameter is 30 for the NLM method.

From the Table 2 we can see that the FPC2 method is as fast as the OSV model, it is about 10 times faster than the NLM method. The SSIM data of the images recovered by the FPC2 method are the highest of the three methods. In terms of SNR, the 'synthetic' image recovered by both the OSV model and the FPC2 method are the same, they are higher than the NLM method, but for the other three test images the FPC2 method has a higher SNR than the other two methods.

Figures 2 shows the images recovered by the three methods and their difference images. From the recovered images, all methods preserve the edges well and avoid the staircase effect. As for the difference images, clear fine edges are almost visible in the difference images of the OSV model, a small amount of geometric structure can be vaguely seen in the difference images of the NLM method, while it is difficult to find geometric information in the difference images of the FPC2 method.

4.3. Comparison of ALM and new fixed point curvature method

With reference to FFTALM [37] and GSALM [38], the augmented Lagrangian Method demonstrates its effectiveness and efficiency in the MC model of $\Phi(\kappa) = |\kappa|$. The method proposed in this study is also applicable to the case of $\Phi(\kappa) = |\kappa|$ with $\mathcal{M}(\nabla u) = \nabla \cdot \frac{\beta}{\sqrt{1+|\nabla u|^2}|\kappa|_\beta^3}\left(\boldsymbol{I} - \frac{\nabla u \nabla u^T}{1+|\nabla u|^2}\right)\nabla$. In this experiment, we compare the recovery efficiency of the FPC2 methods with the FFTALM and GSALM methods for the mean curvature model of $\Phi(\kappa) = |\kappa|$.

The parameter settings for the FFTALM and GSALM methods are $\alpha = 0.45, r_1 = 0.2, r_2 = 42, r_3 = 4 \times 10^3, r_4 = 4.5 \times 10^4$ and the maximum iteration is 400. The α parameters for the FPC2 method of 'Boat', 'Man', 'Dot' and 'Bridge' are 140, 140, 500 and 80 respectively, and $\sigma_0 = 6, \sigma = 2.0$.

Table 3 shows the numerical results of the FFTALM, GSALM and FPC2 methods when processing an image of size 512 × 512 and noise level 20. The data in Table 3 shows that among the three methods, the FCP2 method recovers the highest SNR of the images and requires much less CPU time than the other two methods. For the 'boat', 'Man' and 'Bridge' images, the SSIM of the FPC2 method is significantly higher than that of FFTALM and GSALM, but for the 'Dot' image, the SSIM of the FPC2 method is slightly lower than that of the other two methods.

Figure 3 shows the images recovered by the three methods. From the recovered images, the clouds in the sky, the lines on the mast, and the surface of the water in the 'Boat' image recovered by the FPC2 method are closer to the original image; while in the 'Man' image recovered by the FPC2 method, the girl's arms are recovered more smoothly than in the other two methods, and the dots on the girl's skirt are also recovered better.

5. Conclusions

This paper presents a new fixed point curvature method for solving the Euler-Lagrange equations for the mean curvature model. The method consists of reducing the nonlinearity of $\mathcal{M}(\nabla u)$ by replacing

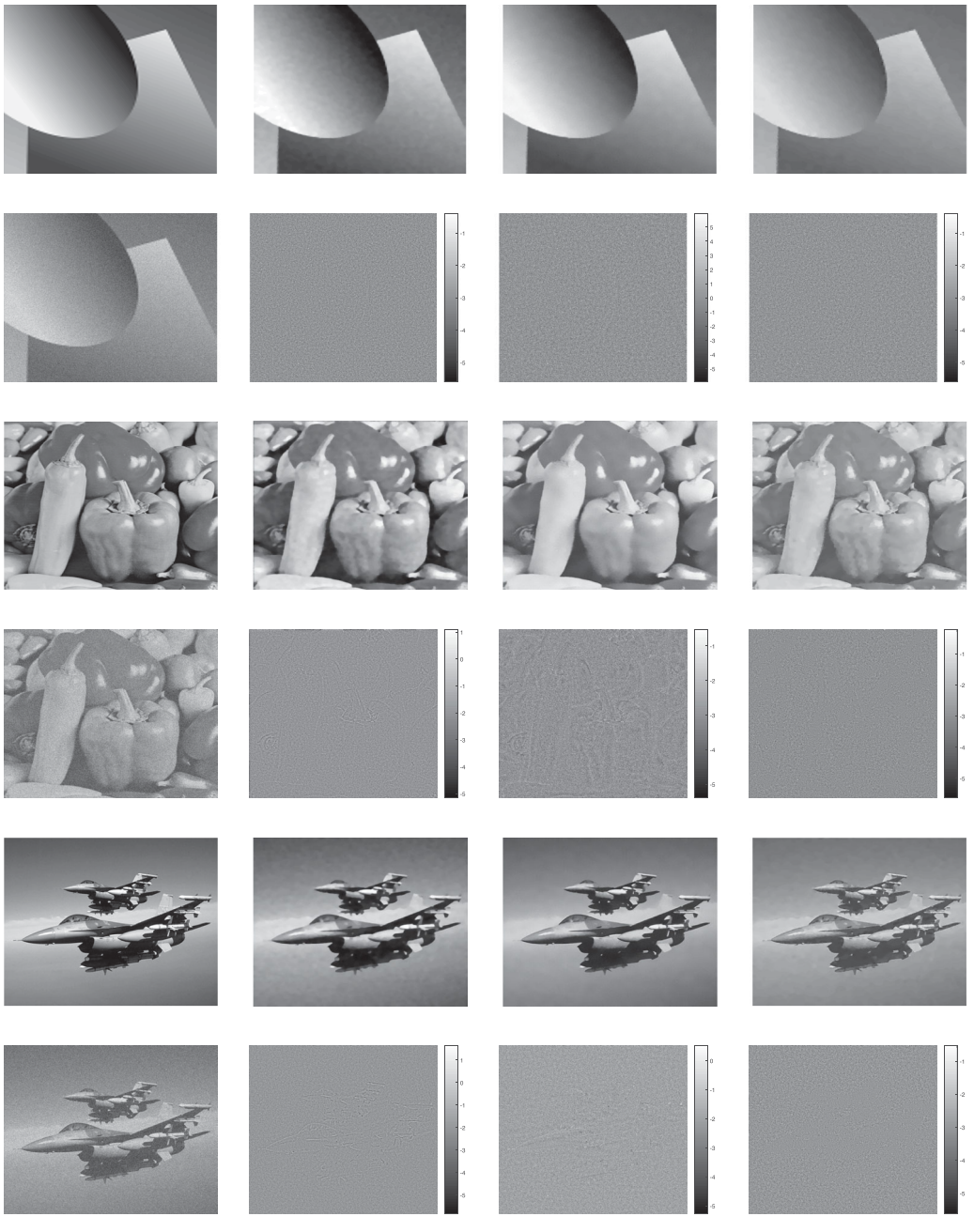

Figure 2. From left column to right column: original 'Pepper' image and noisy image, recovered images and difference images by OSV model, NLM method and FPC2 method.

the gradient ∇u in the second order semi-positive definite operator $\mathcal{M}(\nabla u)$ by $\nabla G_\sigma * u$ to obtain a variant of the Euler-Lagrange equations which is similar in structure to the Euler-Lagrange equation of the OSV model. When the standard deviation of the Gaussian filter is large, the equation is close to the Euler-Lagrange equation of the OSV model. Combined with the fact that the fixed-point method can efficiently solve the Euler-Lagrange equation of the OSV model, we construct the fixed-point curvature iteration method. In addition, for highly noisy images, we introduce a parameter continuation

Table 3. Numerical results for 'Boat', 'Man', 'Dot' and 'Bridge' of size 512 × 512.

Example	Boat			Man		
Method	SNR	SSIM	time	SNR	SSIM	time
FFTALM	25.40	0.9129	192.30	22.55	0.8912	177.36
GSALM	25.33	0.9051	210.15	22.53	0.8823	217.46
FPC2	26.27	0.9244	22.67	22.82	0.8941	29.82
Example	Dot			Bridge		
Method	SNR	SSIM	time	SNR	SSIM	time
FFTALM	31.35	0.9904	184.59	19.78	0.8835	166.90
GSALM	30.61	0.9910	214.16	19.71	0.8701	198.87
FPC2	31.97	0.9875	30.04	19.98	0.8955	28.34

Figure 3. From left column to right column: original images, noisy images, recovered images by FFTALM method, GSALM method and FPC2 method.

procedure to gradually reduce the standard deviation of the Gaussian filtering during the iteration process.

Numerical experiments show that our method recovers the image geometry better, especially the edges, in the same time as the OSV model. It also recovers high quality images from highly noisy images, and the images recovered by our method have higher SNR and SSIM compared to the NLM method, and the speed is 10 times faster than the NLM method. More importantly, our method is not only faster, but also recovers smoother and more natural images with less detail loss than the ALM method that solves the mean curvature model.

Acknowledgments

We are grateful to Professor Wei Zhu for the provision of the source codes of the FFTALM and GSALM methods.

Disclosure statement

No potential conflict of interest was reported by the author(s).

Funding

The research was supported by the National Natural Science Foundation of China (11501243).

References

[1] X. Ai, G. Ni, and T. Zeng, *Nonconvex regularization for blurred images with Cauchy noise*, Inverse Probl. Imaging 16(3) (2022), pp. 625–646.
[2] L. Alvarez, P.-L. Lions, and J. Morel, *Image selective smoothing and edge detection by nonlinear diffusion (II)*, SIAM J. Numer. Anal. 29 (1992), pp. 845–866.
[3] K. Bredies, K. Kunisch, and T. Pock, *Total generalized variation*, SIAM J. Imaging Sci. 3(3) (2010), pp. 492–526.
[4] C. Brito-Loeza and K. Chen, *Multigrid algorithm for high order denoising*, SIAM J. Imaging Sci. 3(3) (2010), pp. 363–389.
[5] A. Buades, B. Coll, and J. Morel, *A review of image denoising algorithms, with a new one*, SIAM Multiscale Model. Simul. 4(2) (2005), pp. 490–530.
[6] F. Catte, P.-L. Lions, J.-M. Morel, and T. Coll, *Image selective smoothing and edge detection by nonlinear diffusion*, SIAM J. Numer. Anal. 29(1) (1992), pp. 182–193.
[7] T. Chan, H. Zhou, and R. Chan, *Advanced signal processing algorithms*, in *Proceedings of the International Society of Photo-Optical Instrumentation Engineers*, F.T. Luk, ed., SPIE, 1995, pp. 314–325.
[8] T.F. Chan, G.H. Golub, and P. Mulet, *A nonlinear primal-dual method for total variation-based image restoration*, SIAM J. Sci. Comput. 20(6) (1999), pp. 1964–1977.
[9] T.F. Chan, A. Marquina, and P. Mulet, *High-order total variation-based image restoration*, SIAM J. Sci. Comput. 22 (2000), pp. 503–516.
[10] T.F. Chan, S.H. Kang, and J. Shen, *Euler's elastica and curvature-based inpainting*, SIAM J. Appl. Math. 63 (2002), pp. 564–592.
[11] L.-J. Deng, R. Glowinski, and X.-C. Tai, *A new operator splitting method for the Euler elastica model for image smoothing*, SIAM J. Imaging Sci. 12(2) (2019), pp. 1190–1230.
[12] Y. Duan, Y. Wang, and J. Hahn, *A fast augmented Lagrangian method for Euler's elastica models*, Numer. Math.: Theory Methods Appl. 6(1) (2012), pp. 47–71.
[13] F. He, X. Wang, and X. Chen, *A penalty relaxation method for image proccessing using Euler's elastica model*, SIAM J. Imaging Sci. 14(1) (2021), pp. 389–417.
[14] K. Jon, J. Liu, X. Wang, W. Zhu, and Y. Xing, *Weighted hyper-Laplacian prior with overlapping group sparsity for image restoration under Cauchy noise*, J. Sci. Comput. 87 (2021), pp. 1–32.
[15] Z. Liu, B. Sun, X.-C. Tai, Q. Wang, and H. Chang, *A fast minimization algorithm for the Euler elastica model based on a bilinear decomposition*, SIAM J. Imaging Sci. 46(1) (2024), pp. 290–314.
[16] X. Lv, F. Li, J. Liu, and S. Lu, *A patch-based low-rank minimization approach for speckle noise reduction in ultrasound images*, Adv. Appl. Math. Mech. 14(1) (2022), pp. 155–180.
[17] M. Lysaker, A. Lundervold, and X.-C. Tai, *Noise removal using fourth-order partial differential equation with applications to medical magnetic resonance images in space and time*, IEEE Trans. Image Process. 12(12) (2003), pp. 1579–1590.
[18] M. Ma and J. Yang, *Poisson image restoration via an adaptive Euler's elastica regularization*, J. Intell. Fuzzy Syst. 45 (2023), pp. 2095–2110.
[19] J.-M. Morel and S. Solimini, *Variational Methods in Image Segmentation*, Progress in Nonlinear Differential Equations and their applications, Birkhäuser Boston, Cambridge, MA, 1995.
[20] S. Osher and J. Sethian, *Fronts propagating with curvature dependant speed: algorithms based on the Hamilton-Jacobi formulation*, J. Comput. Phys. 79 (1988), pp. 12–49.
[21] S. Osher, A. Solé, and L. Vese, *Image decomposition and restoration using total variation minimization and the H^{-1} norm*, SIAM Multiscale Model. Simul. 1(3) (2003), pp. 349–370.
[22] P. Perona and J. Malik, *Scale space and edge detection using anisotropic diffusion*, IEEE Trans. Pattern Anal. Mach. Intell. 12(7) (1990), pp. 629–639.
[23] L.I. Rudin, S. Osher, and E. Fatemi, *Nonlinear total variation based noise removal algorithms*, Physica D 60 (1992), pp. 259–268.
[24] Y. Shi, Q. Chang, and J. Xu, *Convergence of fixed point iteration for deblurring and denoising problem*, Appl. Math. Comput. 189 (2007), pp. 1178–1185.
[25] P. Sonneveld, *CGS: A fast lanczos-type solver for nonsymmetric linear systems*, SIAM J. Sci. Comput.10(1) (1989), pp. 36–52.

[26] X.-C. Tai, J. Hahn, and G.J. Chung, *A fast algorithm for Euler's elastica model using augmented Lagrangian method*, SIAM J. Imaging Sci. 4(1) (2011), pp. 313–344.
[27] V. Torre and T. Poggio, *On edge detection*, IEEE Trans. Pattern Anal. Mach. Intell. 8(2) (1986), pp. 147–163.
[28] C.R. Vogel and M.E. Oman, *Iterative methods for total variation denoising*, SIAM J. Imaging Sci. 17 (1996), pp. 227–238.
[29] Y. Wang and Z. Pang, *Image denoising based on a new anisotropic mean curvature model*, Inverse Probl. Imaging 16(3) (2022), pp. 625–646.
[30] A.P. Witkin, *Scale-space filtering*, in *Proceedings of IJCAI*, Karlsruhe, 1983, pp. 1019–1021.
[31] T. Wu, Y. Min, C. Huang, Z. Li, Z. Wu, and T. Zeng, *An efficient inexact Gauss-Seidel-based algorithm for image restoration with mixed noise*, J. Sci. Comput. 99(2) (2024), pp. 1–28.
[32] F. Yang, K. Chen, and B. Yu, *Homotopy method for a mean curvature-based denoising model*, Appl. Numer. Math. 62 (2012), pp. 185–200.
[33] F. Yang, K. Chen, B. Yu, and D. Fang, *A relaxed fixed point method for a mean curvature-based denoising model*, Optim. Methods Softw. 22(9) (2014), pp. 274–285.
[34] J. Zhang and K. Chen, *A new augmented Lagrangian primal dual algorithm for elastica regularization*, J. Algorithms Comput. Technol. 10(4) (2016), pp. 325–338.
[35] J. Zhang, C. Deng, Y. Shi, S. Wang, and Y. Zhu, *A fast linearised augmented Lagrangian method for a mean curvature based model*, East Asian J. Appl. Math. 8(3) (2018), pp. 463–476.
[36] Q. Zhong, Y. Li, Y. Yang, and Y. Duan, *Minimizing discrete total curvature for image processing*, in *Proceedings of the IEEE/CVF Conference on Computer Vision and Pattern Recognition*, Seattle, 2020, pp. 9471–9479.
[37] W. Zhu, X. Tai, and T. Chan, *Augmented Lagrangian method for a mean curvature based image denoising model*, Inverse Probl. Imaging. 7(1) (2013), pp. 1409–1432.
[38] W. Zhu, X. Tai, and T. Chan, *A fast algorithm for a mean curvature base image denoising model using augmented Lagrangian method*, in *Global Optimization Methods*, LNCS 8293, Springer-Verlag Berlin Heidelberg; 2014, pp. 104–118.
[39] W. Zhu and T. Chan, *Image denoising using mean curvature*, SIAM J. Imaging Sci. 5(1) (2012), pp. 1–32.